Inorganic Chemistry
Article

Inorg. Chem. **2010**, *49*, 6925–6930 **6925**
DOI: 10.1021/ic100491g

Widely Differing Photochemical Behavior in Related Octahedral $\{Ru\text{-}NO\}^6$ Compounds: Intramolecular Redox Isomerism of the Excited State Controlling the Photodelivery of NO

Ariel G. De Candia, Juan P. Marcolongo, Roberto Etchenique, and Leonardo D. Slep*

Departamento de Química Inorgánica, Analítica y Química Física, INQUIMAE, Facultad de Ciencias Exactas y Naturales, Universidad de Buenos Aires−CONICET, Ciudad Universitaria Pabellón 2, 3er Piso, C1428EHA Buenos Aires, Argentina

Received March 15, 2010

trans-$[(NC)Ru(py)_4(\mu\text{-}CN)Ru(py)_4(NO)]^{3+}$ (py = pyridine) is a stable species in aqueous solution. It displays an intense absorption in the visible region of the spectrum (λ_{max} = 518 nm; ε_{max} = 6100 M^{-1} cm^{-1}), which turns this compound into a promising agent for the photodelivery of NO. The quantum yield for the photodelivery process resulting from irradiation with 455 nm visible light was found experimentally to be $(0.06 \pm 0.01) \times 10^{-3}$ mol einstein^{-1}, almost 3 orders of magnitude smaller than that in the closely related *cis*-$[RuL(NH_3)_4(\mu\text{-}pz)Ru(bpy)_2(NO)]^{5+}$ species (L = NH_3 or pyridine, pz = pyrazine, bpy = 2,2′-bipyridine; ϕ_{NO} = 0.02−0.04 mol einstein^{-1} depending on L) and also much smaller than the one in the mononuclear compound *trans*-$[ClRu(py)_4(NO)]^{2+}$ ($\phi_{NO} = (1.63 \pm 0.04) \times 10^{-3}$ mol einstein^{-1}). DFT computations provide an electronic structure picture of the photoactive excited states that helps to understand this apparently abnormal behavior.

Introduction

Transition metal nitrosyl compounds have become the focus of many studies during the last 20 years once the physiological role of nitric oxide was unraveled.[1] These apparently simple molecules are fascinating systems that display diverse reactivity modes, depending on the coordination geometry and overall electron counting at the $\{M-NO\}^n$ fragment.[2] The electronic structure and properties of several group 8 octahedral species with $n = 6$ are compatible with an $M^{II}-NO^+$ limiting electronic description.[3] The interaction of these species with light in the solid state at low temperature has been described since the 1970s. These studies triggered the discovery of the light-induced linkage isomerism of the metal nitrosyl bond.[4] The activity in this field has been remarkable, and nowadays the family of compounds displaying this sort of behavior has grown to several dozens, including examples with other metal centers and electronic configurations.[5−7] On the basis of recent estimations,[7] ∼80% of all known nitrosyl species with $n = 6$ are probably involved in photoinduced linkage-isomerism processes.

In (aqueous) solution, $\{M-NO\}^6$ species are also known to get implicated in photochemical processes but of a different kind, leading to the photodissociation of a neutral nitric oxide molecule and the formation of an M(III) solvento species, as in eq 1.[8,9]

$$[X_5M-NO]^n \xrightarrow[+H_2O]{h\nu} [X_5M-OH_2]^n + NO^{\bullet} \qquad (1)$$

*To whom correspondence should be addressed. E-mail: slep@qi.fcen.uba.ar.

(1) (a) Ignarro, J. L. *Nitric Oxide in Biology and Photobiology*; Academic Press: San Diego, CA, 2000. (b) Stamler, J. S.; Singel, D. J.; Loscalzo, J. *Science* **1992**, *258*, 1898–1902. (c) Richter-Addo, G. B.; Legzdins, P. *Metal Nitrosyls*; Oxford University Press: New York, 1992.

(2) (a) Enemark, J. H.; Feltham, R. D. *Coord. Chem. Rev.* **1974**, *13*, 339–406. (b) Enemark, J. H.; Feltham, R. D. *Top. Stereochem.* **1981**, *12*, 155–215. (c) Olabe, J. A.; Slep, L. D. Reactivity and Structure of Complexes of Small Molecules: Nitric and Nitrous Oxide. In *Comprehensive Coordination Chemistry II, from Biology to Nanotechnology*; Mc Cleverty, J. A., Meyer, T. J., Eds.; Elsevier: Oxford, U.K., 2004; Vol. *1*, pp 603−623.

(3) Roncaroli, F.; Videla, M.; Slep, L. D.; Olabe, J. A. *Coord. Chem. Rev.* **2007**, *251*, 1903–1930.

(4) (a) Carducci, M. D.; Pressprich, M. R.; Coppens, P. *J. Am. Chem. Soc.* **1997**, *119*, 2669–2678. (b) Coppens, P.; Fomitchev, D. V.; Carducci, M. D.; Culp, K. *J. Chem. Soc., Dalton Trans.* **1998**, 865–872.

(5) (a) Fomitchev, D. V.; Furlani, T. R.; Coppens, P. *Inorg. Chem.* **1998**, *37*, 1519–1526. (b) Cheng, L.; Novozhilova, I.; Kim, C.; Kovalevsky, A.; Bagley, K. A.; Coppens, P.; Richter-Addo, G. B. *J. Am. Chem. Soc.* **2000**, *122*, 7142–7143. (c) Kim, C.; Novozhilova, I.; Goodman, M. S.; Bagley, K. A.; Coppens, P. *Inorg. Chem.* **2000**, *39*, 5791–5795. (d) Boulet, P.; Chermette, H.; Weber, J. *Inorg. Chem.* **2001**, *40*, 7032–7039. (e) Coppens, P.; Novozhilova, I.; Kovalevsky, A. *Chem. Rev.* **2002**, *102*, 861–883. (f) Guida, J. A.; Ramos, M. A.; Piro, O. E.; Aymonino, P. J. *J. Mol. Struct.* **2002**, *609*, 39–46. (g) Kovalevsky, A. Y.; Bagley, K. A.; Coppens, P. *J. Am. Chem. Soc.* **2002**, *124*, 9241–9248. (h) Kovalevsky, A. Y.; Bagley, K. A.; Cole, J. M.; Coppens, P. *Inorg. Chem.* **2003**, *42*, 140–147.

(6) Boulet, P.; Buchs, M.; Chermette, H.; Daul, C.; Furet, E.; Gilardoni, F.; Rogemond, F.; Schlapfer, C. W.; Weber, J. *J. Phys. Chem. A* **2001**, *105*, 8999–9003.

(7) Bitterwolf, T. E. *Coord. Chem. Rev.* **2006**, *250*, 1196–1207.

(8) (a) Wolfe, S. K.; Swinehart, J. H. *Inorg. Chem.* **1975**, *14*, 1049–1053. (b) De Leo, M.; Ford, P. C. *J. Am. Chem. Soc.* **1999**, *121*, 1980–1981. (c) Adachi, H.; Sonoki, H.; Hoshino, M.; Wakasa, M.; Hayashi, H.; Miyazaki, Y. *J. Phys. Chem. A* **2001**, *105*, 392–398. (d) Togniolo, V.; da Silva, R. S.; Tedesco, A. C. *Inorg. Chim. Acta* **2001**, *316*, 7–12. (e) Videla, M.; Braslavsky, S. E.; Olabe, J. A. *Photochem. Photobiol. Sci.* **2005**, *4*, 75–82.

(9) Tfouni, E.; Krieger, M.; McGarvey, B. R.; Franco, D. W. *Coord. Chem. Rev.* **2003**, *236*, 57–69.

Published on Web 06/25/2010

It has not been until recently that the advantages of using coordination species behaving as cage compounds for the photodelivery of biomolecules were acknowledged.[10,11] Coordination compounds are thermally stable; they can be designed to display high extinction coefficients in the visible region of the spectrum and high quantum yields for the photodissociation process. The ubiquitous role of NO in many biochemical processes together with the photochemical reactivity described by eq 1 for $\{M-NO\}^6$ species fueled-up the work with nitrosyl containing transition metal complexes in pharmacology.[9,11,12] Unluckily, most of the $\{M-NO\}^6$ group 8 octahedral species normally display absorption profiles shifted to the UV region of the spectrum because of the stabilization of the metal centered orbitals that arises from strong metal−nitrosyl π-interactions. This feature precludes to some extent the use of these molecules with living tissues that are sensitive and opaque to irradiation with low wavelength light sources. Two approaches are described in the literature to cope with this complication: substitution of the metal centers to explore other electronic configurations[13] or modifications of the coordination sphere of the $\{M-NO\}^6$ complexes to broaden the absorption spectrum to the visible region.[14] This can be performed by means of conjugated heterocyclic ligands that can act as light antennae or employing a second metal center that introduces long-range charge-transfer excited states.[15,16] We focus here on this last alternative. A recent set of publications[15,16] describes the photodelivery of an NO molecule from a set of pyrazine bridged dinuclear species of general formula *cis*-$[RuL(NH_3)_4(\mu\text{-pz})Ru(bpy)_2(NO)]^{5+}$ (pz = pyrazine, bpy =2,2′-bipyridine, L = pyridine or NH_3 (compound $\mathbf{1}^{5+}$)). These compounds display quantum yields for the photodelivery of NO (ϕ_{NO}) close to 0.03−0.04 mol einstein^{-1} depending on L and red-shifted absorption profiles with high molar absorbance in the visible region. In these reports,[15,16] the lowest energy excited state responsible for the experimentally found photochemical behavior was tentatively described as one of the two possible electronic isomers *cis*-$[Ru^{II}L(NH_3)_4(\mu\text{-pz})Ru^{III}(bpy)_2(NO^{\bullet})]^{5+}$ or *cis*-$[Ru^{III}L(NH_3)_4(\mu\text{-pz})Ru^{II}(bpy)_2(NO^{\bullet})]^{5+}$.

Some time ago, some of us reported the preparation and characterization of *trans*-$[(NC)Ru(py)_4(\mu\text{-CN})Ru(py)_4(NO)]^{3+}$ (py = pyridine, $\mathbf{2}^{3+}$).[17] This dinuclear complex displays an intense absorption in the visible region (λ_{max} = 518 nm, $\varepsilon_{518} = 6100\ M^{-1}\ cm^{-1}$) arising from a charge transfer process involving $[Ru(py)_4(CN)_2]$ as the donor fragment and $[Ru(py)_4(NO)]^{3+}$ as the acceptor. We now explored the photochemical release of NO in our CN-bridged species. To our surprise, and despite the similarities with the pz-bridged species, we measured a rather small $\phi_{NO} \approx 10^{-5}$ mol einstein^{-1}, even when the mononuclear *trans*-$[ClRu(py)_4(NO)]^{2+}$ species ($\mathbf{3}^{2+}$) itself photoreleases NO much more efficiently (see later). This initially disappointing result prompted us to explore in greater detail the electronic structure of the lowest energy excited state of the dinuclear compounds. Our findings indicate important differences in the electronic distribution and constitute a piece of warning for the future design of NO releasing compounds.

Experimental Section

Materials. The compounds *trans*-$[RuCl(py)_4(NO)](PF_6)_2$ and *trans*-$[(NC)Ru(py)_4(\mu\text{-CN})Ru(py)_4(NO)](PF_6)_3$ were prepared according to previously published procedures[17,18] and fully characterized by IR (KBr pellets), ^{1}H- and ^{13}C-NMR spectroscopies, and elemental analyses. All other reagents employed in this work were obtained commercially and used as supplied.

Physical Determinations. Microanalytical data for C, H, and N were obtained with a Carlo Erba EA 1108 analyzer. IR spectral measurements (KBr pellets) were carried out using alternatively one of two Fourier transform (FT) spectrophotometers, a Nicolet 150P and a Thermo Nicolet AVATAR 320. ^{1}H- and ^{13}C-NMR spectra were measured with a 500 MHz Bruker AM 500 spectrometer. UV−vis spectra were recorded with an HP 8452A diode array spectrophotometer in a gastight stoppered 1 cm path-length quartz cuvette cell. Visible light irradiation of the samples was performed with a 455 nm, 5 mm diameter light-emitting diode (LED) with a spectral half-width of 20 nm. The light power of this source (1.44×10^{-8} einstein s^{-1} cm^{-3}) was calibrated in a test photolysis of *cis*-$[Ru(bpy)_2(py)_2]^{2+}$ (quantum yield of photosubstitution = 0.26).[19]

The quantum yields for the photorelease of nitrogen monoxide were determined by measuring the concentration of NO at low conversion. The quantitative determination was performed with a commercial NO detector (inNO, Nitric Oxide Measuring System, Harvard Apparatus GmbH). The system consisted of an 800 mV potentiostat (TEQ-03) and a combined electrode (700 μm diameter, amino series of nitrogen monoxide sensors). Calibration of the electrode in the range of 10−400 nM was performed by generating NO according to the reaction in eq 2, under an Ar atmosphere

$$H_2SO_4 + NaNO_2 + NaI \rightarrow NO + \frac{1}{2}I_2 + H_2O + Na_2SO_4 \quad (2)$$

For each calibration, aliquots (20 μL) of aqueous $NaNO_2$ (~10 μM) were added to 3.0 mL of a 0.03 M solution of NaI in 0.1 M H_2SO_4. Cronoamperograms were registered at a fixed temperature (25.0 ± 0.1 °C, Lauda RC 20 thermostat) while stirring the solution in order to maintain a constant rate of oxidation of the produced NO at the electrode surface. The typical sensitivity of the electrode was about 170 pA/nM. For the quantum yield determinations, chronoamperograms were

(10) (a) Salierno, M.; Marceca, E.; Peterka, S.; Yuste, R.; Etchenique, R. *J. Inorg. Biochem.* **2010**, *104*, 418–422. (b) Fino, E.; Araya, R.; Peterka, D. S.; Salierno, M.; Etchenique, R.; Yuste, R. *Front. Neural Circuits* **2009**, *3*, 2. (c) Rial Verde, E. M.; Zayat, L.; Etchenique, R.; Yuste, R. *Front. Neural Circuits* **2008** *2*, 2. (d) Zayat, L.; Noval, M. G.; Campi, J.; Calero, C. I.; Calvo, D. J.; Etchenique, R. *ChemBioChem* **2007**, *8*, 2035–2038. (e) Zayat, L.; Salierno, M.; Etchenique, R. *Inorg. Chem.* **2006**, *45*, 1728–1731. (f) Nikolenko, V.; Yuste, R.; Zayat, L.; Baraldo, L. M.; Etchenique, R. *Chem. Commun.* **2005**, 1752–1754. (g) Zayat, L.; Calero, C. I.; Albores, P.; Baraldo, L. M.; Etchenique, R. *J. Am. Chem. Soc.* **2003**, *125*, 882–883.

(11) Rose, M. J.; Mascharak, P. K. *Curr. Opin. Chem. Biol.* **2008**, *12*, 238–244.

(12) Ford, P. C.; Bourassa, J.; Miranda, K.; Lee, B.; Lorkovic, I.; Boggs, S.; Kudo, S.; Laverman, L. *Coord. Chem. Rev.* **1998**, *171*, 185–202.

(13) (a) Eroy-Reveles, A. A.; Leung, Y.; Beavers, C. M.; Olmstead, M. M.; Mascharak, P. K. *J. Am. Chem. Soc.* **2008**, *130*, 4447–4458. (b) Ford, P. C.; Wecksler, S. *Coord. Chem. Rev.* **2005**, *249*, 1382–1395. (c) Hoffman-Luca, C. G.; Eroy-Reveles, A. A.; Alvarenga, J.; Mascharak, P. K. *Inorg. Chem.* **2009**, *48*, 9104–9111.

(14) (a) Halpenny, G. M.; Mascharak, P. K. *Inorg. Chem.* **2009**, *48*, 1490–1497. (b) Rose, M. J.; Mascharak, P. K. *Chem. Commun.* **2008**, 3933–3935. (c) Rose, M. J.; Mascharak, P. K. *Inorg. Chem.* **2009**, *48*, 6904–6917. (d) Rose, M. J.; Olmstead, M. M.; Mascharak, P. K. *Polyhedron* **2007**, *26*, 4713–4718. (e) Rose, M. J.; Patra, A. K.; Alcid, E. A.; Olmstead, M. M.; Mascharak, P. K. *Inorg. Chem.* **2007**, *46*, 2328–2338.

(15) Sauaia, M. G.; de Lima, R. G.; Tedesco, A. C.; da Silva, R. S. *J. Am. Chem. Soc.* **2003**, *125*, 14718–14719.

(16) Sauaia, M. G.; de Lima, R. G.; Tedesco, A. C.; da Silva, R. S. *Inorg. Chem.* **2005**, *44*, 9946–9951.

(17) Roncaroli, F.; Baraldo, L. M.; Slep, L. D.; Olabe, J. A. *Inorg. Chem.* **2002**, *41*, 1930–1939.

(18) Bottomley, F.; Mukaida, M. *J. Chem. Soc., Dalton Trans.* **1982**, 1933–1937.

(19) Pinnick, D. V.; Durham, B. *Inorg. Chem.* **1984**, *23*, 1440.

registered upon irradiation of 3.0 mL of an acidified (HCl 0.01 M) aqueous solution of each complex in steps of 10−120 s. Each experiment was carried out under Ar. During the photolysis measurements, the NO sensor was positioned outside the light path to avoid any photoelectric interference.

Theoretical Calculations. We employed density functional theory (DFT) computations to fully optimize the geometries of the ground singlet and first-excited triplet states of $\mathbf{1}^{5+}$, $\mathbf{2}^{3+}$, and $\mathbf{3}^{2+}$ in vacuum, without symmetry constraints. In order to test some of the conclusions, the computations were also performed on a small set of mononuclear ruthenium-nitrosyl species that also undergo efficient photodissociation of NO, namely, *trans*-$[Ru(pz)(NH_3)_4(NO)]^{3+}$ and *trans*-$[Ru(py)(NH_3)_4(NO)]^{3+}$. We also included *cis*-$[(pz)Ru(bpy)_2(NO)]^{3+}$, a fragment related to $\mathbf{1}^{5+}$. The calculations were carried out with the *Gaussian 03* package,[20] at the B3LYP level of theory using restricted and unrestricted approximations of the Kohn−Sham equations depending on the total number of electrons. In all cases, we employed the effective core potential basis set LanL2DZ, tight SCF convergence criteria, and default settings in the geometry optimizations. This combination proved to be suitable for geometry predictions in other ruthenium centered nitrosyl species.[21,22] The true nature of the stationary points, which correspond to (local) minima in the potential energy surface, was confirmed by numerical vibrational frequency computations. In all cases the absence of negative frequencies confirmed that the optimized geometries correspond to stable configurations in the potential energy surfaces. The spin density of the triplet states was calculated on the basis of the density matrix given by *Gaussian 03*. Time dependent (TD)DFT computations at the ground state equilibrium geometry involving at least 70 singlet and 70 triplet excited states were employed as an assistant tool in the interpretation and assignment of the electronic spectra and photochemical properties.

Further explorations of the potential energy surface (PES) of the triplet states were done using the same functional and level of theory as in the optimization jobs. In each run, the Ru−N bond length was increased in steps of 0.02 to 0.2 Å starting from the equilibrium distance. The rest of the internal degrees of freedom were then fully optimized. The dissociation curves obtained for the different compounds allow us to correlate qualitatively the dissociation energy (D_e) to the photochemical quantum yield determined experimentally.

Results and Discussion

The deeply violet dinuclear compound $\mathbf{2}^{3+}$ owes its color to an intense Gaussian-shaped absorption band ($\lambda_{max} = 518$ nm; $\varepsilon_{max} = 6100\ M^{-1}\ cm^{-1}$, Figure 1). We already reported that this species seems to release NO upon irradiation in the visible region of the spectrum, but only now, and inspired by the photochemical properties of $\mathbf{1}^{5+}$ we decided to examine this process quantitatively. We explored the photochemistry in aqueous solution irradiating at 455 nm on the upper energy side of the absorption band ($\varepsilon_{455} = 3335\ M^{-1}\ cm^{-1}$) and employing low light power to avoid side reactions. The quantum yield for NO-formation (ϕ_{NO}) was obtained by electrochemically sensing the NO produced upon irradiation, a technique already employed with many nitrosyl compounds. This is a simple and fast method for the detection and quantification of the NO in the 10^{-9} M scale, allowing

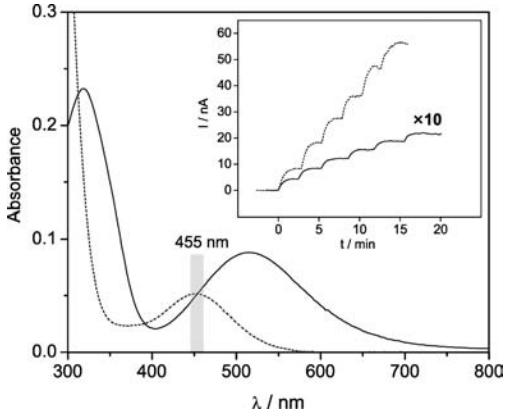

Figure 1. Electronic spectra of $\mathbf{3}^{2+}$ (dashed line) and $\mathbf{2}^{3+}$ (solid line) at the actual concentrations used in the photolysis experiments (3.4×10^{-4} M and 1.5×10^{-5} M in aqueous solution, respectively). Inset: Chronoamperograms for the photorelease of NO of $\mathbf{3}^{2+}$ (dashed line) and $\mathbf{2}^{3+}$ (solid line) upon irradiation steps of 20 s. The typical sensitivity of the NO detector was about 170 pA/nM.

reliable measurements at low conversion. Figure 1 displays the chronoamperogram of NO released by photolysis of a 1.5×10^{-5} M solution of $\mathbf{2}^{3+}$. The experimental ϕ_{NO} result is $(0.06 \pm 0.01) \times 10^{-3}$ mol einstein^{-1}, a value that is surprisingly smaller than the typical ones measured in other $\{RuNO\}^6$.

We attempted to compare this value with the one in $\mathbf{3}^{2+}$, but to our knowledge this system was never studied quantitatively in solution. A recent publication dealing with the light-induced linkage isomerism of $\mathbf{3}^{2+}$ suggested that even in the solid state this compound may undergo photodecomposition, probably due to the photorelease of NO.[23] Therefore we also explored this molecule under the same conditions employed for the dinuclear compound. In this case, the 455 nm irradiation wavelength (see Figure 1) overlaps with a weak absorption band centered at 453 nm ($\varepsilon_{453} = 140\ M^{-1}\ cm^{-1}$). This same transition was observed in acetonitrile solution ($\lambda_{max} = 450$ nm, $\varepsilon_{450} = 150\ M^{-1}\ cm^{-1}$)[24] and ascribed to a metal to ligand $d_{Ru} \rightarrow \pi^*_{NO}$ charge transfer transition (see later). The observed quantum yield for product formation obtained spectroscopically was in this case 30 times higher reaching $(1.63 \pm 0.04) \times 10^{-3}$ mol einstein^{-1}. This value, though still small for any practical applications, lies in the lower end of the usual range observed in other mononuclear $\{RuNO\}^6$ systems,[9,25] suggesting that the $[Ru(py)_4(NO)]^{3+}$ moiety is not responsible by itself for the overall decrease in ϕ_{NO}.

At this point there is a crucial issue that has to be considered in order to explain the differences in the quantum yields of NO photorelease, namely, the electronic description of the lowest energy excited states of the different compounds involved in the primary photochemical process. In the past we have successfully employed density functional theory (DFT) electronic structure calculations to understand the photochemical behavior of $[Ru(bpy)(AN)_4]^{2+}$ (bpy = 2,2′-bipyridyl, AN = acetonitrile).[22] We apply here the same methodology to explore the electronic structure of the three species in an attempt to evaluate

(20) Frisch, M. J. *Gaussian 03*, versions C.02 and D.01, Gaussian Inc.: Wallingford, CT, 2004.
(21) (a) Videla, M.; Jacinto, J. S.; Baggio, R.; Garland, M. T.; Singh, P.; Kaim, W.; Slep, L. D.; Olabe, J. A. *Inorg. Chem.* **2006**, *45*, 8608–8617. (b) De Candia, A. G.; Marcolongo, J. P.; Slep, L. D. *Polyhedron* **2007**, *26*, 4719–4730.
(22) Petroni, A.; Slep, L. D.; Etchenique, R. *Inorg. Chem.* **2008**, *47*, 951–956.
(23) Schaniel, D.; Cormary, B.; Malfant, I.; Valade, L.; Woike, T.; Delley, B.; Kramer, K. W.; Gudel, H. U. *Phys. Chem. Chem. Phys.* **2007**, *9*, 3717–3724.
(24) Coe, B. J.; Meyer, T. J.; White, P. S. *Inorg. Chem.* **1995**, *34*, 593–602.
(25) Rose, M. J.; Mascharak, P. K. *Coord. Chem. Rev.* **2008**, *252*, 2093–2114.

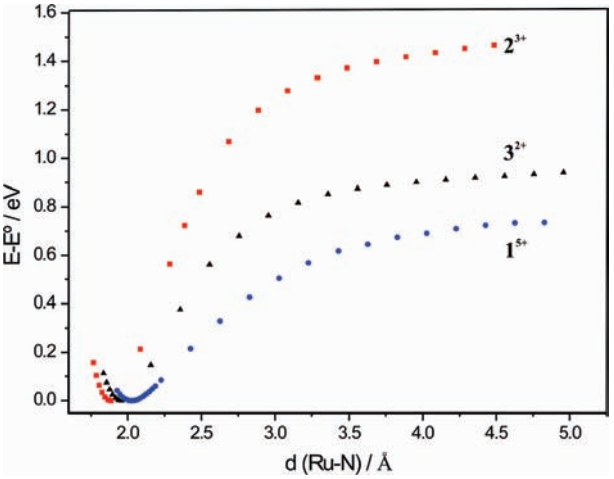

Figure 2. Dissociation curves calculated by DFT for the lowest energy excited triplets of the three compounds ($\mathbf{1}^{5+}$, $\mathbf{2}^{3+}$, and $\mathbf{3}^{2+}$). See the Experimental Section for details in the calculations.

the intrinsic differences between $\mathbf{3}^{2+}$, $\mathbf{2}^{3+}$, and $\mathbf{1}^{5+}$ that justify ϕ_{NO} values that span a 2 orders of magnitude range.

The ground state geometry optimization of the three species renders essentially linear Ru−NO fragments with typical geometrical parameters for octahedral species (Supporting Information). The evaluation of the photochemistry also requires a geometry optimization of the lowest energy excited state and a complementary potential energy surface (PES) scan of the relevant internal coordinates (in this case the Ru−NO bond-length) in order to evaluate the dissociation of the NO moiety.

Figure 2 shows the dissociation curves of the lowest energy triplet states of the three species, calculated in vacuum. The dissociation energy follows the trend $\mathbf{1}^{5+} < \mathbf{3}^{2+} < \mathbf{2}^{3+}$. The strength of the Ru−N bond is also reflected in the excited state computed equilibrium Ru−NO bond-lengths (Supporting Information). Though the energy values are probably overestimated because of the absence of solvent in the computations, the results are still valuable from the qualitative point of view. In this set of compounds it appears that the rupture of the Ru−N bond determines the quantum yield of photorelease. The computed dissociation energy (D_e) in other mononulcear $\{RuNO\}^6$ species known to also undergo efficient photodissociation[9] (see the Supporting Information) are comparable to the values obtained for $\mathbf{1}^{5+}$ and $\mathbf{3}^{2+}$. This suggests that the abnormally low ϕ_{NO} (or high D_e) of $\mathbf{2}^{3+}$ does not originate on a subtle effect but most probably on a large difference in the electronic structure of its photoreactive state.

The photoreactivity of this kind of species has been rationalized in the past as arising from the presumably long-lived lowest energy excited state assumed to be mostly $Ru^{III}-NO^{\bullet}$ in character. Figure 3 collects the relevant frontier orbitals in the three species. In all cases, the main contribution to the lowest unoccupied molecular orbital (LUMO) comes from the nitrosyl π^*_{NO}, with partial delocalization onto the metal centered orbitals. A lowest energy excited state with some degree of charge transfer to the nitrosyl fragment is therefore a reasonable choice to start the analysis. The nature and energy spacing of the highest occupied molecular orbital (HOMO) and other occupied MOs close in energy are, on the contrary, markedly different. This fact will prove determinant when exploring the excited state behavior. In none of the three cases

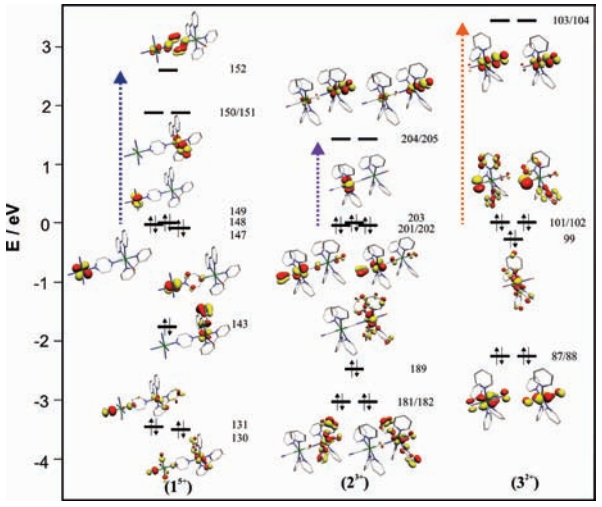

Figure 3. MO diagrams showing the most relevant frontier orbitals for $\mathbf{1}^{5+}$, $\mathbf{2}^{3+}$, and $\mathbf{3}^{2+}$. The arrows identify the main orbital contributions to the lowest energy intensity-carrying electronic transitions. For the sake of clarity, the orbitals that are not relevant to the discussion of the photoreactivity were omitted.

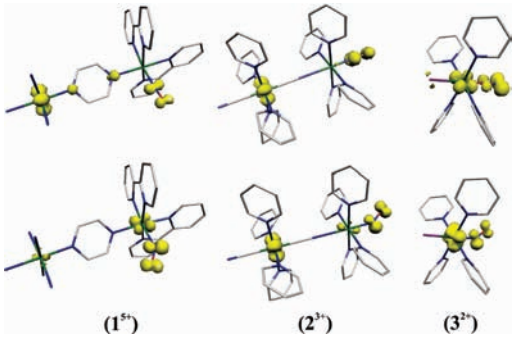

Figure 4. Spin density for the lowest energy triplet states at ground state (top) and at the excited state equilibrium geometry (bottom) of the three compounds ($\mathbf{1}^{5+}$, $\mathbf{2}^{3+}$, and $\mathbf{3}^{2+}$).

the nature of the thermally equilibrated lowest energy excited state is straightforward. We compare here the three cases.

***trans*-[ClRu(py)$_4$(NO)]$^{2+}$.** (TD)DFT computations at the ground state equilibrium geometry suggest that the lowest energy absorption band at 450 nm results from the convolution of two weak charge tranfer transitions. The first one is $d_{Ru} \rightarrow \pi^*_{NO}$ in origin and involves orbitals 99 and 103/104 (calculated $\lambda_{max} = 508$ nm, $f = 0.0015$). The second one corresponds to the HOMO → LUMO transition and can be viewed as a $\pi_{Cl} \rightarrow \pi^*_{NO}$ charge transfer (calculated $\lambda_{max} = 438$ nm, $f = 0.0020$). In any case, intersystem crossing occurring after the absorption of light populates a triplet state, which is mostly $d_{Ru} \rightarrow \pi^*_{NO}$ in origin, as can be seen on a plot of the computed spin density of the lowest excited triplet state at the ground state equilibrium geometry (Figure 4). The orbitally degenerate excited state molecule undergoes a Jahn−Teller distortion[6] that removes the orbital degeneracy and leads to bending of the Ru−NO unit and lengthening of the N−O bond ($\angle_{RuNO}$ 179.5° and $d_{Ru-N} = 1.77$ Å at the ground state (GS) equilibrium geometry; $d_{Ru-N} = 1.95$ Å and $\angle_{RuNO} = 141.6°$ at the minimum of the PES of the ^{3}MLCT state). In parallel with these geometrical changes, the species undergoes electronic rearrangements that influence the total spin density (Figure 4). This geometrical and electronic changes

leave an NO• molecule weakly coordinated to a Ru(III) center. Dissociation of this fragment occurs via further lengthening of the Ru−N bond. We observed the same kind of behavior for the computed lowest energy triplet state of other mononuclear $\{RuNO\}^6$ species (Supporting Information).

***trans*-[(NC)Ru(py)$_4$(μ-CN)Ru(py)$_4$(NO)]$^{3+}$.** The presence of an extra ruthenium center introduces new transitions in the visible region of the spectrum. The lowest energy absorption band responsible of its deep violet color has been tentatively associated to a long-range donor−acceptor charge transfer transition (DACT).[17] A molecular orbital picture built upon DFT electronic structure computations confirms this assignment (Figure 4). The t_{2g} orbital set of the metal centers splits under C_4 symmetry into b_2 and e. The HOMO (orbital 203) is nonbonding, transforms as b_2 and is mostly located on the dicyano fragment. Immediately below in energy is a first set of degenerate e orbitals essentially centered on the same fragment (orbitals 201 and 202). The LUMO is located on the other end of the molecule and is largely π^*(NO) in character (orbitals 204 and 205). Both $b_2 \rightarrow e$ and $e \rightarrow e$ transitions are symmetry allowed. However, the orientation of the b_2 orbital of the dicyano fragment makes the former transition overlap forbidden, leaving a unique assignment for the strong visible band. The lowest energy triplet state at the GS equilibrium geometry still arises from a long distance CT but involving a different metal orbital on the donor fragment. Both (TD)DFT and single point computations of the triplet state show that this state is actually $b_2 \rightarrow e$ in character. Jahn−Teller distortion during the lifetime of the excited state leads to lengthening of the Ru−NO bond and bending of the Ru−NO angle. The computed relaxed triplet state geometry shows an NO molecule coordinated to a Ru^{II} center and not to a Ru^{III} as in $\mathbf{3}^{2+}$. A comparison between the computed dissociation energies for lowest energy triplet states of $\mathbf{2}^{3+}$ and $\mathbf{3}^{2+}$ (Figure 2) shows a more weakly bounded neutral NO molecule in the latter. This result is not completely unexpected, provided that the extra electron in the $\{Ru^{II}-NO^{\bullet}\}$ moiety of $\mathbf{2}^{3+}$ (absent in the $\{Ru^{III}-NO^{\bullet}\}$ fragment of $\mathbf{3}^{2+}$) is associated with a π-bonding molecular orbital, or in other words the π-backdonation arising from a Ru^{II} metal center is more efficient than in a Ru^{III} species. In view of the molecular orbital picture, the electronic distribution for the lowest energy triplet excited state is in this case better described as *trans*-[(NC)-Ru^{III}(py)$_4$(μ-CN)Ru^{II}(py)$_4$($NO^{\bullet}$)]$^{3+}$. In this description, the NO ligand sits in an essentially equivalent environment than the one that results from a $1e^-$ reduction of the $\{RuNO\}$ fragment to yield a $\{Ru^{II}NO\}^7$ moiety. The actual $1e^-$ reduced species $\mathbf{2}^{2+}$ has been thoroughly characterized.[17] The spectroscopic evidence supports a *trans*-[(NC)Ru^{II}(py)$_4$-(μ-CN)Ru^{II}(py)$_4$($NO^{\bullet}$)]$^{2+}$ formulation, with a non-labile $\{Ru^{II}-NO^{\bullet}\}^7$ fragment. As a matter of fact, recent studies have shown that NO• compounds of +2 metal centers with a low spin d^6 electronic configuration can be much more inert than expected. For instance, the rate constant for the dissociation of NO• in $[Fe(CN)_5NO]^{3-}$ has been reported to be $(1.58 \pm 0.06) \times 10^{-3}\ s^{-1}$.[26] The activation enthalpy reported in this case was $\Delta H^{\ddagger} = 106.4 \pm 0.8$ kJ mol^{-1}.

***cis*-[(H$_3$N)$_5$Ru(μ-pz)Ru(bpy)$_2$(NO)]$^{5+}$.** Analogously to the case discussed above, the second ruthenium center becomes responsible for the richer electronic spectroscopy. (TD)DFT computations performed at the ground state geometry in vacuo indicate that the strong absorption in the visible region of the spectrum, observed experimentally at 530 nm, is better described as a $d_{\pi}((H_3N)_5$-$Ru^{II}) \rightarrow \pi^*_{pz}$ MLCT (λ_{calcd} = 449 nm; f = 0.420). The electronic distribution of this state can therefore be described as *cis*-[$(H_3N)_5Ru^{III}(\mu$-$pz^{\bullet -})Ru^{II}(bpy)_2(NO)]^{5+}$. However, the lowest energy excited triplet state displays a completely different electronic distribution, better described as *cis*-[$(H_3N)_5Ru^{III}(\mu$-pz)$Ru^{II}(bpy)_2(NO^{\bullet})]^{5+}$ (Figure 4). This is the outcome of electronic isomerism processes typically associated with ground-state mixed-valence systems, which can also occur between electronically coupled excited states of comparable energy. Also in this case, the Ru−NO fragment distorts during the lifetime of the excited state to yield a minimum in the PES. In parallel with the geometrical changes, one electron is transferred from the $Ru^{II}(bpy)_2(NO^{\bullet})$ to the distant $(H_3N)_5Ru^{III}$ leading to a *cis*-[$(H_3N)_5Ru^{II}(\mu$-pz)Ru^{III}-$(bpy)_2(NO^{\bullet})]^{5+}$species whose spin density is displayed in Figure 4. After this somewhat cumbersome series of interconvertions between excited state electronic isomers, this species ends up with a $\{Ru^{III}-NO^{\bullet}\}$ fragment similar geometrically and electronically to the one responsible for NO photoliberation in $\mathbf{3}^{2+}$. It is not strange therefore that this compound displays a ϕ_{NO} value of (0.025 ± 0.002) mol einstein^{-1} at 532 nm.[15]

Conclusions

The use of DFT computations helped to understand the low value of ϕ_{NO} in $\mathbf{2}^{3+}$. On the basis of the previous experience with other dinuclear systems, this compound appeared as a promising cage compound for the photorelease of NO: it holds an octahedral $\{RuNO\}^6$ fragment, it is extremely inert toward thermal decomposition, and it has a strong absorption band in the visible region of the spectrum. We have shown that the presence of a second Ru center, though responsible for the increase in the extinction coefficient, introduces uncertainty in the prediction of the electronic distribution upon light absorption. This situation does not always lead to a lowest energy excited state with the appropriate electronic distribution to favor the release of a neutral NO molecule. The example described in this work and our interpretation show that the approach based on coupling of metallic fragments to a knowingly photoreactive nitrosyl carrying center to enhance its spectral properties may not always lead to success. At the same time, the high ϕ_{NO} values reported in the literature for a series of *cis*-[$RuL(NH_3)_4(\mu$-pz)Ru-$(bpy)_2(NO)]^{5+}$ species are the clear demonstration that the overall strategy can also be successful. Nevertheless, the election of the appropriate fragment combination might not be trivial. Electronic structure computations may eventually assist in this task.

Acknowledgment. The authors thank the University of Buenos Aires (UBA), the Consejo Nacional de Investigaciones Científicas y Técnicas (CONICET), the Agencia Nacional de Promoción Científica y Tecnológica (ANPCyT), and Fundación Antorchas (Argentina) for funding. This work was partially supported by the

(26) Roncaroli, F.; Olabe, J. A.; van Eldik, R. *Inorg. Chem.* **2003**, *42*, 4179–4189.

National Center for Supercomputing Applications under Grant TG-MCA05S010. L.D.S. and R.E. are members of the scientific staff of CONICET, and A. G.D.C. and J.P.M. are postdoctoral and graduate fellows from CONICET, respectively.

Supporting Information Available: Tables with relevant structural information and figures showing the DFT optimized structures for the compounds discussed in this work. This material is available free of charge via the Internet at http://pubs.acs.org.